Optimizing Single-Cell Long-Read Sequencing for Enhanced Isoform Detection in Pancreatic Islets

Running title: Single-cell Long-Read Sequencing in Pancreatic Islets

Maria S. Hansen, Christopher J. Hill, Lori Sussel, Kristen L. Wells*

Barbara Davis Center, University of Colorado Anschutz Medical Campus, Aurora CO 80045

*Corresponding Author: Kristen.wells-wrasman@cuanschutz.edu

Keywords: single cell long read RNA-sequencing, transcriptomics, islet biology, RNA isoforms, RNA splicing

Word count: 4,218

Figures: 3

Tables: 4

Abstract

Alternative splicing is an essential mechanism for generating protein diversity by producing distinct isoforms from a single gene. Dysregulation of splicing that affects pancreatic function and immune tolerance has been linked to both type 1 and type 2 diabetes. Next-generation sequencing technologies, with their short read lengths, are limited in their ability to accurately detect splice variants. Long-read sequencing technologies offer the potential to overcome these limitations by providing full-length transcript information; however, their application in single-cell RNA sequencing has been hindered by technical challenges, including insufficient read lengths and higher error rates. Furthermore, cell types that produce high levels of a single transcript, such as islet endocrine cells, can obscure identification of lower abundance transcripts. In this study, we optimized a protocol for single-cell long-read sequencing in pancreatic islets to improve read length and transcript detection. Our findings demonstrate that 5' library preparation protocols outperform 3' protocols, resulting in better transcript identification. Furthermore, we show that targeted depletion of insulin transcripts enhances the detection of informative reads, highlighting the utility of transcript depletion strategies. This optimized protocol enables isoform-specific gene expression analysis and reveals differential transcript usage across the various cell types in pancreatic islets. By leveraging this approach, we gain deeper insights into the transcriptomic complexity and cellular heterogeneity within pancreatic islets.

Article Highlights

- This study addresses the limitations of current single-cell long-read RNA-sequencing (sclrRNA-seq) technologies in detecting full-length transcripts and isoform diversity, particularly in pancreatic islets.
- We demonstrate that optimizing single-cell library preparation protocols reproducibly enhances read length and transcript identification in pancreatic islets.
- 5' capture methods, combined with targeted insulin depletion and extended reverse transcription, significantly improved read length and isoform detection compared to standard protocols, while maximizing the number of informative reads.
- These improvements yield longer reads in single-cell experiments, substantially enhancing transcript identification and enabling more accurate analysis of isoform diversity.

Introduction

Alternative splicing (AS) plays a critical role in generating protein diversity from the ~22,000 known protein-coding genes, leading to the production of over 140,000 distinct transcripts [1]. This process allows for the generation of proteins with different amino acid sequences, impacting their functions and localization within the cell, and allowing them to respond readily to changes in the environment [2, 3]. Splicing dysregulation is a key factor in many diseases, including diabetes, either due to inherent mutations in splice sites or RNA-binding proteins (RBPs), or in response to changes in environmental conditions, such as inflammatory stress or hyperglycemia [4, 5]. In the context of type 1 diabetes (T1D), diversity in isoform expression has significant implications for pancreatic function and immune

67 tolerance. For example, differential isoform expression of autoantigens IA-2 and G6pc2
68 between the pancreas and thymus has been proposed to contribute to the generation of
69 autoreactive T cells in T1D [6, 7]. Furthermore, dysregulated splicing events have been
70 observed in islets from individuals with type 2 diabetes (T2D), underscoring the importance
71 of splicing regulation in maintaining proper cellular function and immune homeostasis [5].
72 As one specific example, SNAP-25, a component of the SNARE complex responsible for
73 vesicle fusion and exocytosis, exists as two isoforms (SNAP-25a and SNAP-25b). In SNAP-
74 25b-deficient mice, [Ca^{2+}] elevations are prematurely activated and delayed in termination,
75 and insulin secretion is increased [8].

76 Despite the critical need to detect splice variants in the context of diabetes, next
77 generation sequencing (NGS) technologies remain insufficient for this task. Identifying
78 isoform-specific gene expression requires sequencing reads that span multiple exons of the
79 mRNA transcript. In the human genome, transcript lengths are estimated to average
80 between 1,800 and 4,900 bp, with the mode of the distribution around 2,000 bp [9]. NGS
81 technologies have read lengths of 150 base pairs, making it difficult to identify isoforms. In
82 contrast, long-read sequencing technologies, such as PacBio and Oxford Nanopore
83 Technologies, offer the generation of full-length reads that can capture the full RNA
84 molecule, thereby providing a clearer picture of isoform diversity. Published single-cell long-
85 read RNA sequencing (sclrRNA-seq) libraries often report shorter read lengths than
86 expected, which may limit transcript coverage and isoform detection. For instance, a recent
87 study reported a median read length of 900 bp for sclrRNA-seq of two cancer cell lines [10].

88 Advances in sequencing technologies, especially single-cell approaches, have
89 revealed the complex heterogeneity within the pancreas, uncovering distinct functional and
90 transcriptomic subpopulations across different cell types. In pancreatic islets, single-cell
91 genomics and patch-seq have identified transcriptionally and functionally distinct beta-cell
92 subpopulations directly linking gene expression to key physiological processes such as
93 vesicle exocytosis [11]. This heterogeneity underscores the importance of characterizing
94 splicing events and their resulting isoforms at the single-cell level. However, sclrRNA-seq
95 technologies come with inherent limitations. Nanopore flow cells produce fewer reads than
96 Illumina, with around 20,000 reads per cell for a 5,000-cell experiment, well below the
97 typical 30,000–50,000 reads per cell common in NGS. Moreover, Nanopore's higher error
98 rate (1%) increases the likelihood of incorrect barcode and UMI assignments. To overcome
99 these challenges, we have optimized a protocol for pancreatic islets that improves read
100 length, advancing the utility of long-read sequencing for single-cell transcriptomics.
101

102 **Research Design and Methods**

103 **Dissociation of pancreatic islets**

104 10-week-old female C57BL/6 mice were obtained from Jackson laboratories.
105 Pancreatic islets were isolated from mice under ketamine/xylazine/acepromazine
106 anesthesia by collagenase delivery into the pancreas via injection into the bile duct. The
107 collagenase-inflated pancreas was surgically removed and digested. After isolation, islets
108 were dissociated using Accutase in a 37°C bead bath for 25-30 minutes. Single-cell
109 suspension was filtered through a 40 mm filter and quenched in RPMI media + 10% FBS.

110 Cells were washed again with RPMI +10% FBS and with PBS + 0.1% BSA. Single-cell
111 suspensions were loaded into a Genomics Chromium targeting 4000 cells per sample.

112 **Dissociation of spleens**

113 Spleens were isolated from mice under ketamine/xylazine/acepromazine
114 anesthesia. Spleens were dissociated through a 70 µm strainer in cIMDM using a 3 mL
115 syringe plunger. Cells were washed, centrifuged, and treated with 1 mL Ammonium-
116 Chloride-Potassium (ACK) lysis buffer for 30 seconds, followed by dilution in cIMDM and a
117 second spin. After one additional cIMDM wash, cells were resuspended in PBS + 0.1% BSA.
118 Single-cell suspensions were loaded into a Genomics Chromium targeting 4000 cells per
119 sample.

120 **scRNA-seq library preparation and insulin depletion**

121 Single-cell libraries were prepared using either the Chromium Next GEM Single Cell
122 3' Kit v3.1 or the Chromium Next GEM Single Cell 5' Kit v2 following the protocol up to and
123 including step 2.4, stopping just before fragmentation. For the optimized libraries, the
124 following modifications were applied to the 5' library preparation: 1 ul 10 mM dNTP solution
125 (Thermo Scientific FERR0191) was added to the reaction in step 1.1. The extension time was
126 increased from 45 minutes to 2 hours in step 1.5. 1 ul 10 mM dNTP solution was added to
127 the reaction in step 2.2 and the extension time was increased from 1 minute to 3 minutes.
128 Insulin depletion was performed on cDNA from step 2.4 of the 10X Genomics Chromium
129 library preparation using the DepleteX™ RNA Depletion Panel (Insulin) kit from Jumpcode
130 Genomics. We followed the PacBio MAS-IsoSeq protocol (December 2022, Version 1.0) with
131 the following modifications: During RNP Complex Formation (Step A), we used 0.9 ul Cas9

132 instead of 2.3 ul, and 1.6 ul Insulin Guide RNA instead of 4.0 ul Single Cell Boost Guide RNA.
133 During Bead Cleanup (Step D), we used 50 ul (1X) AMPure XP Beads instead of 75 ul 1.5X
134 SMRTbell Cleanup Beads.

135 Following insulin depletion, long-read libraries were prepared from the cDNA using
136 Sequencing Kit V14 (Nanopore SQK-LSK114) and the PCR Expansion (Nanopore EXP-
137 PCA001). For 3' libraries, the *Ligation sequencing V14 — single-cell transcriptomics with 3'*
138 *cDNA prepared using 10X Genomics on PromethION (SQK-LSK114)* protocol was used. For
139 5' libraries, the *Ligation sequencing V14 - Single-cell transcriptomics with 5' cDNA prepared*
140 *using 10X Genomics on PromethION (SQK-LSK114)* protocol was used. Short Fragment
141 Buffer (SFB) was used for library preparation instead of Long Fragment buffer (LFB). Library
142 Beads (LIB) were used for the flow cell priming mix stead of Library Solution (LIS). Libraries
143 were sequenced on R10.4.1 flow cells on either a PromethION 2 Solo (P2S) or PromethION
144 2 Integrated (P2i).

145 **Bulk RNA-seq library preparation**

146 Islets were isolated from two male C57BL/6J mice as described above. RNA was
147 purified using the Qiagen RNeasy micro kit (Qiagen Cat # 74004). Bulk RNA-seq libraries
148 were prepared using KAPA mRNA Hyper Prep kit (Roche 8098123702), following the KAPA
149 mRNA HyperPrep Kit protocol (KR1352 – v7.21). Insulin depletion was applied between step
150 8 and 9 in the KAPA library prep protocol.

151 **Single-cell RNA-seq preprocessing**

152 Single-cell libraries were processed using the EPI2ME single-cell workflow v1.1.0
153 from Oxford Nanopore Technologies for the identification of cell and UMI barcodes

154 (https://github.com/epi2me-labs/wf-single-cell) using the mm10-2020-A mouse reference
155 provided by 10x Genomics. The kit name was either 3prime or 5prime depending on the 10x
156 library preparation and we provided the kit version v3 and v1 for the 3' and 5' samples we
157 prepared respectively. We provided the kit version that was indicated in the publications
158 associated with each published dataset. All parameters can be found on github
159 (https://github.com/CUAnschutzBDC/sc-islet-longread-
160 analysis/blob/61d52b6ef94ff974a394a9335dd65d28b9e6360e/01_wf_single_cell/trial_par
161 ameters.tsv) The pipeline was altered to bypass the StringTie step to use a consistent GTF
162 file from the mm10 genome. These jobs were executed using Singularity and Nextflow. Only
163 the reads that had a sequence quality higher than 7 were input into this pipeline.

164 We manually created a gene count matrix from the BAM outputs that were produced
165 by the EPI2ME pipeline, and then utilized the emptyDrops function from the DropletUtils
166 package [12] to identify cell barcodes. Using these barcodes, we subset the gene and
167 transcript count matrices from the single-cell workflow and calculated the read lengths of
168 cells that were identified using the barcodes. Read lengths were calculated from the BAM
169 files by looking at the length of the query sequences for all primary reads and were subset
170 further by matching barcodes (CB), whether the read was tagged with a gene (GN), and
171 whether the read was tagged with a transcript (TR). Finally, we examined the BAM files and
172 calculated the number of reads that were tagged with a gene and a transcript, before creating
173 the final output plots.

174 **Detailed analysis of the 5' modified islet dataset**

The filtered data for the 5' modified islet dataset was input into Seurat (v4.1.3) [13-17], using R (v4.2.3). Quality control metrics were calculated using the perCellQCMetrics function from the Scuttle package (v1.8.4) [18]. We used the DoubletFinder package (v2.0.3) [19] to remove cells that were identified as doublets, before running PCA. We tested several resolutions of UMAP before generating final clustering.

Cell types were initially identified using a reference dataset [20] and further refined based on the expression of known islet cell type markers. Dimensionality reduction and clustering was first performed using gene-level expression data, followed by a second round of clustering based on transcript-level expression. To evaluate the consistency between gene- and transcript-based cell type annotations, we calculated concordance between the two methods and visualized the results as confusion matrices using the Matrix (v1.5-4) [21] and pheatmap (v1.0.12) packages. Clusters identified by transcript-level expression were used for downstream analysis. To assess differential splicing, we conducted pseudobulk differential transcript usage (DTU) analysis using DTUrtle (v1.0.2) [22] alongside pseudobulk differential gene expression (DGE) analysis. Pseudobulk count matrices were generated by aggregating counts per replicate and cell type using Seurat. Differential expression was tested at the gene level using DESeq2 (v1.38.3), and differential transcript usage was tested at the transcript level using DTUrtle with sparseDRIMSeq (v0.1.2) for model fitting. Batch effects across replicates were corrected using ComBat-seq from the sva package (v3.50.0). Most figures were generated using the dplyr (v1.1.0), ggplot2 (v3.4.1), readr (v2.1.4), tidyverse (v2.0.0), MetBrewer (v0.2.0), and scAnalysisR (v0.0.0.9000) [23] packages. Further details of this pipeline can be found at our code repository:

197 https://github.com/CUAnschutzBDC/maria_long_read_081224/

198 Docker images can be found here:

199 RNA-seq preprocessing (STAR, Fastqc, cutadapt, featurecounts):

200 https://hub.docker.com/r/kwellswrasman/rnaseq_general

201 scRNA-seq (DTurtle, scAnalysisR, Seurat):

202 https://hub.docker.com/r/kwellswrasman/sclrseq_methods_r_docker

203 **Bulk RNA-seq analysis**

204 Raw reads were trimmed using cutadapt (v4.8) and python (v3.10.14) [24] and aligned
205 to the mouse GRCm38 genome using STAR (v2.7.11b) [25]. Gene expression was quantified
206 with featureCounts (v2.0.6) [26] and differential expression analysis was conducted using
207 DESeq2 (v1.44.0) [27] with R version 4.4.1. All plots were made using ggplot2 (v3.5.1) in R.

208 **NGS coverage**

209 The 10k Human DTC Melanoma, Chromium GEM-X Single Cell 5' and 10k Human DTC
210 Melanoma, Chromium GEM-X Single Cell 3' aligned bam files were downloaded from 10x
211 genomics (https://www.10xgenomics.com/datasets). Coverage plots were generated using
212 NGS plot (v2.63) [28].

213 **Transcript Coverage**

214 To visualize the transcript coverage for each of our samples, we utilized the coverage
215 function from the GenomicFeatures (v1.60.0) package. The reads output from our single-cell
216 post-processing pipeline were aligned to a transcriptome reference generated from the
217 GRCm38 Ensembl GTF, and subset based on matching barcodes and unique UMIs from our
218 processed Seurat objects. For each sample, a coverage matrix of counts per transcript

219 position was created for every transcript in the GTF file, then each normalized to be a length
220 of 100. The counts were then normalized by read depth, and then again by applying a softmax
221 transformation to generate matrix values that summed to 1 across each transcript, before a
222 column mean provided a value per each 1-100 position per sample. These coverages were
223 subset based on the number of exons per transcript, supplied by the GTF file, as well as the
224 length of the transcripts, with a prerequisite that the transcript have >1 exon.

225 **Gviz plots**

226 For visualizing our transcriptome-aligned reads on the genome, we utilized Gviz
227 (v1.52.0) and the bam files output from our single-cell post-processing pipeline. Briefly,
228 reads for each sample were aligned to a transcriptome reference generated using the
229 GRCm38 Ensembl GTF file, and subsequently subset based on matching barcodes and
230 unique UMIs from our processed Seurat objects. The final output bam files were generated
231 by subsetting the genome-aligned bam files to only those reads that uniquely mapped to one
232 transcript in our transcriptome alignment. These bams were then merged by replicate. For
233 each of these merged bam files, an alignments track was created utilizing Gviz and displayed
234 alongside the GRCm38 transcripts.

235 **Overrepresentation analysis (ORA)**

236 Differential transcript usage (DTU) genes were subjected to KEGG pathway
237 overrepresentation analysis (ORA) using gprofiler2 (v0.2.1) [29] with a custom background of
238 all expressed genes. KEGG pathways were extracted from the enrichment results and ranked
239 by p-value. The top 25 pathways were visualized as bubble plots.

240 **3' versus 5' bias plot**

241 Isoform-defining splice junctions were identified across datasets. Transcripts were
242 classified based on whether their unique junctions fell in the 3' region (last 25% of the
243 transcript), 5' region (first 25% of the transcript), central (middle 50% of the transcript) or
244 both 5' and 3', and binned accordingly
245
246 **Data availability**
247 All data will be made available on GEO upon publication.
248
249 **Code Availability**
250 All source data supporting the findings of this study are provided. Custom analysis pipelines
251 are available on GitHub at:
252 https://github.com/CUAnschutzBDC/sc-islet-longread-analysis.
253
254 **Results**
255 Evaluation of read lengths and isoform detection in published single-cell long read datasets
256 We aimed to identify isoform differences between islet cell types and subtypes using
257 single-cell RNA-sequencing. To evaluate the ability of single-cell sequencing technologies
258 to generate full-length reads, we reanalyzed previously published sclrRNA-seq datasets
259 generated using 10x Genomics and Oxford Nanopore Technologies, focusing on their ability
260 to capture full-length transcripts and detect isoform-specific transcript expression. Our
261 analysis included seven sclrRNA-seq libraries from five different studies [10, 30-33]. The
262 reanalysis revealed an average read length of 794 bp, and an average mode of 582 bp,

263 compared to the expected mode distribution of ~2,000 bp in the human genome [9] (Figure
264 1A). This discrepancy between the average read length and the expected transcript length
265 underscores the ongoing challenge of capturing full-length transcripts. This shortfall in read
266 length is important because it limits the transcript detection ability. Where gene detection
267 ranges from 60-75% of total reads, transcript detection ranges from 30-60% of total reads
268 (Figure 1B). These findings highlight the limitations of current sclrRNA-seq technologies in
269 achieving comprehensive transcript-level resolution.

270 Efficient and specific depletion of insulin from islet sequencing libraries generates
271 enhanced read diversity

272 Analyzing transcript expression requires a higher overall read depth than gene
273 expression analysis, as each gene is associated with multiple transcripts. Initial analysis of
274 our sclrRNA-seq libraries of mouse pancreatic islets led to the discovery that the two mouse
275 insulin genes, *Ins1* and *Ins2* made up 25% of the total reads, impeding our ability to achieve
276 optimal read depth (Figure 1C). To overcome this issue, we incorporated an insulin depletion
277 step into the protocol and validated the specificity and efficiency of the depletion in a bulk
278 short-read RNA-sequencing library of mouse pancreatic islets. The depletion was
279 remarkably efficient and highly specific: insulin transcripts were uniquely depleted, while all
280 other genes remained unaffected (Figure 1D and Supplementary Table 1). The same insulin
281 depletion was then applied to a single-cell pancreatic islet library followed by long-read
282 Nanopore sequencing. Importantly, the insulin depletion was as efficient as in the bulk
283 sample (Figure 1C). This strategy was applied to all subsequent pancreatic islet libraries
284 generated for this study. Notably, the classification of beta cells does not rely on the

285 presence of insulin transcripts. We demonstrate this by computationally removing insulin
286 reads from a scRNA-seq library and repeating cell clustering (Supplementary Figure 1A-D).
287 Protocol modifications enhance read length and transcript identification in islet single-cell
288 long read libraries
289 Most high-throughput sclrRNA-seq methods rely on 10x Genomics single-cell
290 capture and library preparation, which was originally optimized to generate and amplify
291 shorter sequences, raising the question of whether it can effectively amplify full-length
292 transcripts. 10x Genomics offers two types of transcriptomic profiling for single-cell RNA-
293 seq: one that captures the 3' end of transcripts and another that captures the 5' end. Studies
294 have shown that 3' RNA libraries frequently contain internal priming artifacts [34] that would
295 prevent the amplification of full length reads. To test for internal priming in 3' vs 5' libraries,
296 we downloaded libraries generated using each technology in human melanoma samples
297 from datasets created by 10x Genomics and analyzed the genomic coverage [28]. 3' libraries
298 exhibited a notably higher degree of internal priming compared to 5' libraries, as evidenced
299 by an increased number of reads mapping to the central regions of transcripts in genomic
300 coverage plots (Figure 1E). Because reads generated through internal priming cannot span
301 the full length of a transcript, this phenomenon likely contributes to the shorter read lengths
302 observed in these libraries. To test this, sclrRNA-seq libraries were prepared from mouse
303 pancreatic islets in parallel using both 3' and 5' capture technologies (n = 2 independent
304 biological replicates per capture method). The libraries prepared with 5' technology resulted
305 in a subtle increase in longer reads, compared to the 3' libraries (one-sided Wilcoxon test, p
306 $< 2 \times 10^{-16}$) (Figure 1F and Supplementary Figure 2B). Furthermore, the 5' library provided

307 substantially improved transcript identification, increasing from 46.4 ± 0.1% to 59.7 ± 1.3%
308 (Figure 1B).

309 To further improve the read length, several additional optimization steps were
310 introduced into the islet 5' library preparation protocol (Chromium Next GEM Single Cell 5'
311 Reagent Kits v2), including increasing the extension time from 45 minutes to 2 hours during
312 GEM-RT Incubation and from 1 to 3 minutes during cDNA amplification, based on the
313 approach outlined by Lebrigand et al. [30] and increasing the amount of dNTPs. These
314 modifications resulted in longer reads than those from the 5' library without modifications
315 (one-sided Wilcoxon test, $p < 2 \times 10^{-16}$) (Figure 1F and Supplementary Figure 2B) and enabled
316 far better transcript identification than any of the published datasets (62.0 ± 1.2%; Figure
317 1B). Additionally, the 5' modified libraries showed improved transcript coverage (Figure 1G
318 and Supplementary Figure 2C), with the most pronounced improvement observed in longer
319 transcripts (Figure 1H and Supplementary Figure 2D). Overall, this emphasizes the
320 preference for 5' capture over 3' capture and highlights the necessity for library prep
321 optimizations to enhance the amplification of full-length reads.

322 Isolating high-quality RNA from pancreatic islets is notoriously difficult, primarily due
323 to the presence of digestive enzymes, including RNases that are secreted by the exocrine
324 pancreas. To explore whether a different cell type might yield still longer reads, we applied
325 3', 5', and 5' optimized library preparations, as described above, to lymphocytes isolated
326 from dissociated mouse spleens (n = 2 independent biological replicates per capture
327 method). The 5' lymphocyte samples demonstrated better transcript identification
328 compared to the 3' pancreatic islet samples (Supplementary Figure 2A). However, the 10x

329 Genomics Chromium library prep modifications for the 5’ samples did not yield the same
330 improvements in the lymphocyte samples as observed with the pancreatic islet samples
331 (Supplementary Figure 2A, E-F). This suggests that the benefits of these optimizations might
332 be tissue-specific and highlights the need for further refinements tailored to different tissue
333 types.

334 Isoform variants identified between alpha and beta cells and within beta cell
335 subpopulations

336 With the improved library preparation, the optimized 5’ sclrRNA-seq datasets from
337 mouse pancreatic islets were used to explore whether splicing changes could be detected
338 from different cell types and cell states. Importantly, the 5' modified sclrRNA-seq dataset,
339 merged across replicates, allowed clear identification of all expected cell populations
340 (Figure 2A-B and Supplementary Table 2). Importantly, despite depletion ~95% of insulin
341 transcripts, enough transcripts remain to identify insulin-expressing cells (Figure 2B).
342 Furthermore, the analysis revealed that cell type identification remains robust whether using
343 gene-level or transcript-level expression data for dimensionality reduction and clustering,
344 with over 90% concordance between the two approaches (Figure 2D-G). This stability in
345 broad cell type classification aligns with the understanding that major cell types are defined
346 by distinct gene expression patterns. However, when examining substructure within these
347 cell types, substantial differences emerged between gene-level and transcript-level
348 analyses, with consistency ranging from 43% to 90% across subclusters (Figure 2I,
349 Supplementary Figure 3). These findings suggest that while gene-level expression is
350 sufficient for identifying major cell types, transcript-level analysis provides crucial insights

351 into subtle variations within cell populations. Such variations may reflect different cell
352 states, functions, or responses that are not captured by gene-level analysis alone.

353 The primary strength of sclrRNA-seq lies in its ability to capture cell-specific isoform
354 expression. To assess differential splicing, we performed pseudobulk differential transcript
355 usage (DTU) analysis on merged 5' modified replicates, alongside pseudobulk differential
356 gene expression (DGE) analysis. A pseudobulk approach was chosen because it treats the
357 biological sample, rather than individual cells, as the unit of replication, reducing pseudo-
358 replication and yielding more robust and reproducible results [35, 36]. DTU analysis [22]
359 identifies proportional differences in the transcript composition of a gene, comparing how
360 much each transcript contributes to the total gene expression across conditions. Using this
361 analysis, 218 DTU events were identified between alpha and beta cells (Figure 3A). We also
362 detected 2,095 DGE genes, of which 56 overlapped between the DTU and DGE analyses
363 (Supplementary Table 3). As a representative example of beta cell subpopulation analysis,
364 we focused on the comparison between the 1_beta and 4_beta subpopulations, where we
365 identified 316 DGE genes and 9 DTU genes, with 2 genes overlapping between the two
366 analyses (Supplementary Table 4). Overrepresentation analysis (ORA) of DTU genes revealed
367 enrichment in pathways such as synaptic vesicle cycle, calcium reabsorption, and oxidative
368 phosphorylation in both alpha versus beta cells and 1_beta versus 4_beta comparisons
369 (Figure 3B and Supplementary Figure 4A). Specifically, when comparing alpha and beta
370 cells, we identified isoform-specific differences in *Gnas*, a key regulator of cAMP signaling
371 and insulin secretion (Figure 3C and Supplementary Figure 4B). Additional DTU genes of
372 interest in this comparison include *Pcsk2*, which encodes a prohormone convertase

373 required for insulin processing, as well as *Prdx2*, and *Calm2*, which contribute to antioxidant
374 defense and calcium signaling, respectively. Analysis of two beta cell subpopulations
375 (1_beta and 4_beta) revealed distinct isoform usage of *Ndufs2***,** a central component of
376 oxidative phosphorylation and ATP production (Figure 3D and Supplementary Figure 4C).
377 This comparison also highlighted isoform differences in *Stxbp1***,** a gene important for insulin
378 granule exocytosis. To assess whether 3' or 5' library preparation introduces bias in detecting
379 transcript isoforms, such as preferential capture of variation near the transcript ends, we
380 examined transcript identification based on splice junctions (Supplementary Figure 4D).
381 This analysis showed that there was limited 3' or 5' bias, with differences largely driven by a
382 few highly expressed transcripts. Representative gene plots illustrate that 5' libraries
383 generally provide reads spanning more exon junctions (Supplementary Figure 5), whereas 3'
384 libraries better detect certain long transcripts with substantial 3' end variation
385 (Supplementary Figure 6) and may disproportionately enhance detection of some
386 transcripts due to internal priming (Supplementary Figure 7).
387

388 **Discussion**

389 This study demonstrates how an improved sclrRNA-seq library preparation protocol
390 from isolated islets produces longer reads and increases the proportion of reads that can be
391 confidently assigned to specific transcripts, improving the utility of long-read sequencing
392 data for identifying splice variants and cellular heterogeneity in pancreatic endocrine cell
393 populations. Specifically, this study demonstrates that islet sclrRNA-seq libraries prepared
394 with 5’ protocols outperform those prepared with 3’ protocols. While neither library type

395 showed a strong overall 3' or 5' bias, 3' libraries are prone to internal priming, whereas 5'
396 reads tend to cover more exon junctions, providing more complete isoform identification.
397 Enhancements to the 5’ library preparation further improves read length and transcript
398 tagging efficiency in pancreatic islets. Furthermore, depleting insulin transcripts from the
399 pancreatic islet libraries proved to be a highly effective strategy for maximizing informative
400 reads, demonstrating the broader potential of targeted transcript depletion in single-cell
401 RNA-sequencing experiments.

402 While the modified 5' protocol significantly improved read length in islet samples,
403 lymphocyte samples showed significant improvement only with the unmodified 5' protocol,
404 with no additional benefit from the modifications. This indicates that individual cell types will
405 require unique modifications and further optimizations. Despite the significant
406 improvements in read length achieved with the modified protocol, it did not meet
407 expectations for full-length transcript coverage. Achieving this goal will require further
408 modifications to the 10x chemistry, including adjustments to the master mix and reverse
409 transcriptase.

410 Although full-length coverage was not achieved for all transcripts, we successfully
411 analyzed transcript expression and identified differential transcript usage across cell types
412 and cell subpopulations. These advancements are critical for uncovering the full complexity
413 of transcriptomes and hold immense potential for broad application across tissues,
414 enabling deeper insights into cellular heterogeneity, isoform regulation, and functional
415 diversity. While scRNA-seq allows the identification of distinct cell populations and
416 subpopulations, the precise number and composition of clusters can be influenced by

417 analytical choices such as clustering resolution, preprocessing, and dimensionality
418 reduction, supporting previous analyses showing that subpopulations may not be
419 consistently defined across studies [37]. In addition, transcript capture and read depth can
420 influence subpopulation detection: while adequate coverage suffices for gene-level
421 conclusions, even greater depth is needed to resolve transcript-level differences, as each
422 gene is often associated with multiple transcripts. Despite these limitations, single-cell
423 transcriptomic analyses still provide valuable insights into isoform-level regulation within
424 specific cell types. Investigating these variations at the single-cell level allows us to uncover
425 the intricate heterogeneity within tissues, offering a deeper understanding of the functional
426 and transcriptional diversity that would otherwise go unnoticed. Understanding splicing
427 dysregulation in pancreatic islets is particularly important, as it may reveal how alternative
428 splicing shapes beta cell function, immune tolerance, and beta cell susceptibility in
429 diabetes.
430

431 **Acknowledgments**

432 We thank Laura White, PhD, and Jay Hesselberth, PhD, for their guidance and support with
433 Nanopore long-read sequencing technologies. We thank Mia Smith, PhD, for guidance on
434 spleen sample preparation. We also thank Scott Beard, BDC Cytometer Core Manager, for
435 islet and spleen isolations.
436 **Funding.** This work was supported by grants from the National Institutes of Health
437 (P30DK116073 [Lori Sussel] , R01 DK082590 [Lori Sussel], and U01 DK127505 [Lori Sussel]).
438 **Duality of interest.** No potential conflicts of interest relevant to this article were reported.

Author Contributions. M.S.H. was responsible for data acquisition and prepared the original manuscript. K.L.W. and L.S. reviewed and edited the manuscript. C.J.H. and K.L.W. developed the computational pipelines. M.S.H., C.J.H., and K.L.W. contributed to data analysis and the graphical presentation of results. All authors contributed to the study's methodology and conceptualization. K.L.W. is the guarantor of this work and had full access to all data in the study and takes responsibility for the integrity of the data and the accuracy of the data analysis.

References

1. Gonzalez-Porta, M., et al., *Transcriptome analysis of human tissues and cell lines reveals one dominant transcript per gene.* Genome Biol, 2013. **14**(7): p. R70.
2. Black, D.L., *Mechanisms of alternative pre-messenger RNA splicing.* Annu Rev Biochem, 2003. **72**: p. 291-336.
3. Piazzi, M., et al., *Alternative Splicing, RNA Editing, and the Current Limits of Next Generation Sequencing.* Genes (Basel), 2023. **14**(7).
4. Juan-Mateu, J., O. Villate, and D.L. Eizirik, *MECHANISMS IN ENDOCRINOLOGY: Alternative splicing: the new frontier in diabetes research.* Eur J Endocrinol, 2016. **174**(5): p. R225-38.
5. Jeffery, N., et al., *Cellular stressors may alter islet hormone cell proportions by moderation of alternative splicing patterns.* Hum Mol Genet, 2019. **28**(16): p. 2763-2774.
6. Diez, J., et al., *Differential splicing of the IA-2 mRNA in pancreas and lymphoid organs as a permissive genetic mechanism for autoimmunity against the IA-2 type 1 diabetes autoantigen.* Diabetes, 2001. **50**(4): p. 895-900.
7. Dogra, R.S., et al., *Alternative splicing of G6PC2, the gene coding for the islet-specific glucose-6-phosphatase catalytic subunit-related protein (IGRP), results in differential expression in human thymus and spleen compared with pancreas.* Diabetologia, 2006. **49**(5): p. 953-7.
8. Daraio, T., et al., *SNAP-25b-deficiency increases insulin secretion and changes spatiotemporal profile of Ca(2+)oscillations in beta cell networks.* Sci Rep, 2017. **7**(1): p. 7744.
9. Lopes, I., et al., *Gene Size Matters: An Analysis of Gene Length in the Human Genome.* Front Genet, 2021. **12**: p. 559998.
10. Shiau, C.K., et al., *High throughput single cell long-read sequencing analyses of same-cell genotypes and phenotypes in human tumors.* Nat Commun, 2023. **14**(1): p. 4124.
11. Camunas-Soler, J., et al., *Patch-Seq Links Single-Cell Transcriptomes to Human Islet Dysfunction in Diabetes.* Cell Metab, 2020. **31**(5): p. 1017-1031 e4.
12. Lun, A.T.L., et al., *EmptyDrops: distinguishing cells from empty droplets in droplet-based single-cell RNA sequencing data.* Genome Biol, 2019. **20**(1): p. 63.
13. Hao, Y., et al., *Dictionary learning for integrative, multimodal and scalable single-cell analysis.* Nat Biotechnol, 2024. **42**(2): p. 293-304.
14. Hao, Y., et al., *Integrated analysis of multimodal single-cell data.* Cell, 2021. **184**(13): p. 3573-3587 e29.
15. Stuart, T., et al., *Comprehensive Integration of Single-Cell Data.* Cell, 2019. **177**(7): p. 1888-1902 e21.
16. Butler, A., et al., *Integrating single-cell transcriptomic data across different conditions, technologies, and species.* Nat Biotechnol, 2018. **36**(5): p. 411-420.
17. Satija, R., et al., *Spatial reconstruction of single-cell gene expression data.* Nat Biotechnol, 2015. **33**(5): p. 495-502.

488 18. McCarthy, D.J., et al., *Scater: pre-processing, quality control, normalization and*
489 *visualization of single-cell RNA-seq data in R*. Bioinformatics, 2017. **33**(8): p. 1179-
490 1186.
491 19. McGinnis, C.S., L.M. Murrow, and Z.J. Gartner, *DoubletFinder: Doublet Detection in*
492 *Single-Cell RNA Sequencing Data Using Artificial Nearest Neighbors*. Cell Syst,
493 2019. **8**(4): p. 329-337 e4.
494 20. Baron, M., et al., *A Single-Cell Transcriptomic Map of the Human and Mouse*
495 *Pancreas Reveals Inter- and Intra-cell Population Structure*. Cell Syst, 2016. **3**(4): p.
496 346-360 e4.
497 21. Jagan, D.B.a.M.M.a.M. *Matrix: Sparse and Dense Matrix Classes and Methods*. 2024;
498 Available from: https://CRAN.R-project.org/package=Matrix.
499 22. Tekath, T. and M. Dugas, *Differential transcript usage analysis of bulk and single-cell*
500 *RNA-seq data with DTUrtle*. Bioinformatics, 2021. **37**(21): p. 3781-3787.
501 23. Wells, K.L., et al., *Combined transient ablation and single-cell RNA-sequencing*
502 *reveals the development of medullary thymic epithelial cells*. Elife, 2020. **9**.
503 24. Martin, M., *Cutadapt removes adapter sequences from high-throughput sequencing*
504 *reads*. EMBnet. journal, 2011. **17**(1): p. 10-12.
505 25. Dobin, A., et al., *STAR: ultrafast universal RNA-seq aligner*. Bioinformatics, 2013.
506 **29**(1): p. 15-21.
507 26. Liao, Y., G.K. Smyth, and W. Shi, *featureCounts: an efficient general purpose*
508 *program for assigning sequence reads to genomic features*. Bioinformatics, 2014.
509 **30**(7): p. 923-30.
510 27. Love, M.I., W. Huber, and S. Anders, *Moderated estimation of fold change and*
511 *dispersion for RNA-seq data with DESeq2*. Genome Biol, 2014. **15**(12): p. 550.
512 28. Shen, L., et al., *ngs.plot: Quick mining and visualization of next-generation*
513 *sequencing data by integrating genomic databases*. BMC Genomics, 2014. **15**: p.
514 284.
515 29. Raudvere, U., et al., *g:Profiler: a web server for functional enrichment analysis and*
516 *conversions of gene lists (2019 update)*. Nucleic Acids Res, 2019. **47**(W1): p. W191-
517 W198.
518 30. Lebrigand, K., et al., *High throughput error corrected Nanopore single cell*
519 *transcriptome sequencing*. Nat Commun, 2020. **11**(1): p. 4025.
520 31. Tian, L., et al., *Comprehensive characterization of single-cell full-length isoforms in*
521 *human and mouse with long-read sequencing*. Genome Biol, 2021. **22**(1): p. 310.
522 32. Wang, Q., et al., *Single cell transcriptome sequencing on the Nanopore platform*
523 *with ScNapBar*. RNA, 2021. **27**(7): p. 763-70.
524 33. You, Y., et al., *Identification of cell barcodes from long-read single-cell RNA-seq with*
525 *BLAZE*. Genome Biol, 2023. **24**(1): p. 66.
526 34. Svoboda, M., H.R. Frost, and G. Bosco, *Internal oligo(dT) priming introduces*
527 *systematic bias in bulk and single-cell RNA sequencing count data*. NAR Genom
528 Bioinform, 2022. **4**(2): p. lqac035.
529 35. Zimmerman, K.D., M.A. Espeland, and C.D. Langefeld, *A practical solution to*
530 *pseudoreplication bias in single-cell studies*. Nat Commun, 2021. **12**(1): p. 738.

36. Squair, J.W., et al., *Confronting false discoveries in single-cell differential expression*. Nat Commun, 2021. **12**(1): p. 5692.
37. Mawla, A.M. and M.O. Huising, *Navigating the Depths and Avoiding the Shallows of Pancreatic Islet Cell Transcriptomes*. Diabetes, 2019. **68**(7): p. 1380-1393.

Figure legends

Figure 1

Read length and transcript identification comparison between single-cell long-read RNA-sequencing (sclrRNA-seq) libraries. (A) Read length distribution of published sclrRNA-seq libraries prepared with 10x Genomics and Nanopore technology. Biological replicates are included for datasets from Lebrigand et al., 2020 and Wang et al., 2021; other datasets are shown as single samples. (B) Proportion of reads across datasets where the gene is identified, the transcript is identified, or neither is identified. Shown are published reanalyzed datasets and six mouse pancreatic islet samples: two replicates prepared with 3' 10x Genomics technology, two replicates with 5' 10x Genomics technology, and two replicates with 5' modified 10x Genomics technology (incorporating library preparation optimizations). (C) Proportion of reads aligned to *Ins1* or *Ins2* in a single-cell RNA-seq analysis of mouse pancreatic islets pre- and post-insulin depletion. (D) Volcano plot depicting differential gene expression between non-depleted and insulin-depleted bulk RNA-seq libraries from mouse pancreatic islets. A total of 23,431 genes is shown in the plot. (E) NGS coverage plot indicating read start sites across the genomic region. Libraries shown are 3' and 5' single-cell 10x Genomics preparations derived from human DTC melanoma cells. (F) Read length distribution comparison across mouse pancreatic islet sclrRNA-seq libraries, including two replicates prepared with 3' 10x Genomics technology, two replicates

557 with 5' 10x Genomics technology, and two replicates with 5' modified 10x Genomics
558 technology. (G) Coverage plot showing Softmax-normalized read coverage across relative
559 transcript positions for all multi-exon transcripts in mouse pancreatic islet scRNA-seq
560 libraries prepared with 3', 5', or 5' modified 10x Genomics technology. (H) Coverage plot
561 showing Softmax-normalized read coverage across relative transcript positions for all
562 transcripts with ≥9 exons in mouse pancreatic islet scRNA-seq libraries prepared with 3', 5',
563 or 5' modified 10x Genomics technology.
564
565 Figure 2
566 Comparison of single-cell clustering based on gene expression versus transcript-level
567 expression. (A) UMAP projection of single cells from insulin-depleted mouse pancreatic islet
568 sclrRNA-seq libraries prepared with 5' modified 10x Genomics technology (two biological
569 replicates merged), based on gene-level expression. Cells are colored by gene expression
570 profiles reflecting major pancreatic cell types. (B) Heatmap showing expression of cell type-
571 specific markers across single cells insulin-depleted 5' modified libraries (two biological
572 replicates merged), based on gene-level clustering. (C) UMAP projection of single cells
573 based on gene-level expression, colored by gene expression profiles reflecting cell
574 subpopulations. (D) UMAP projection of single cells based on transcript-level (isoform)
575 expression. Colored by transcript expression profiles reflecting major pancreatic cell types.
576 (E) UMAP projection of single cells based on transcript-level expression, colored by
577 transcript expression profiles reflecting cell subpopulations. (F) Confusion matrix showing
578 concordance in cell type identification between gene-based and transcript-based

clustering. (G) Bar plot quantifying cell type concordance between clustering methods. (H) Confusion matrix showing low concordance in beta cell subpopulation identification between clustering methods. (I) Bar plot quantifying beta cell subpopulation concordance between clustering methods. C1–C5 indicate comparison 1 through comparison 5.

Figure 3

Differential transcript usage between cell types and cell subpopulations. (A) Heatmap showing differential transcript usage (DTU) between alpha and beta cells. Each row represents a transcript (significant at FDR < 0.05), and each column represents a cell type. Colors indicate the fraction of a gene's expression contributed by each transcript within each cell type. DTU genes were identified from pseudobulk analysis of two biological replicates of mouse pancreatic islet sclrRNA-seq libraries prepared with 5' modified 10x Genomics technology. (B) KEGG pathway overrepresentation analysis (ORA) for DTU genes between alpha and beta cells. The x-axis shows recall, i.e., the proportion of functionally annotated genes in the query that are associated with each pathway. Bubble size represents the number of DTU genes in the pathway, and bubble color indicates statistical significance (-log10 p-value). The top 25 enriched KEGG pathways are shown. (C) Differential gene expression (DGE), differential transcript expression (DTE), and differential transcript usage (DTU) analysis of *Gnas* between alpha and beta cells. DTU shows the relative contribution of each transcript to the gene's overall expression. (C) DGE, DTE, DTU analysis of *Ndufs2* between beta cell subpopulations 1_beta and 4_beta.

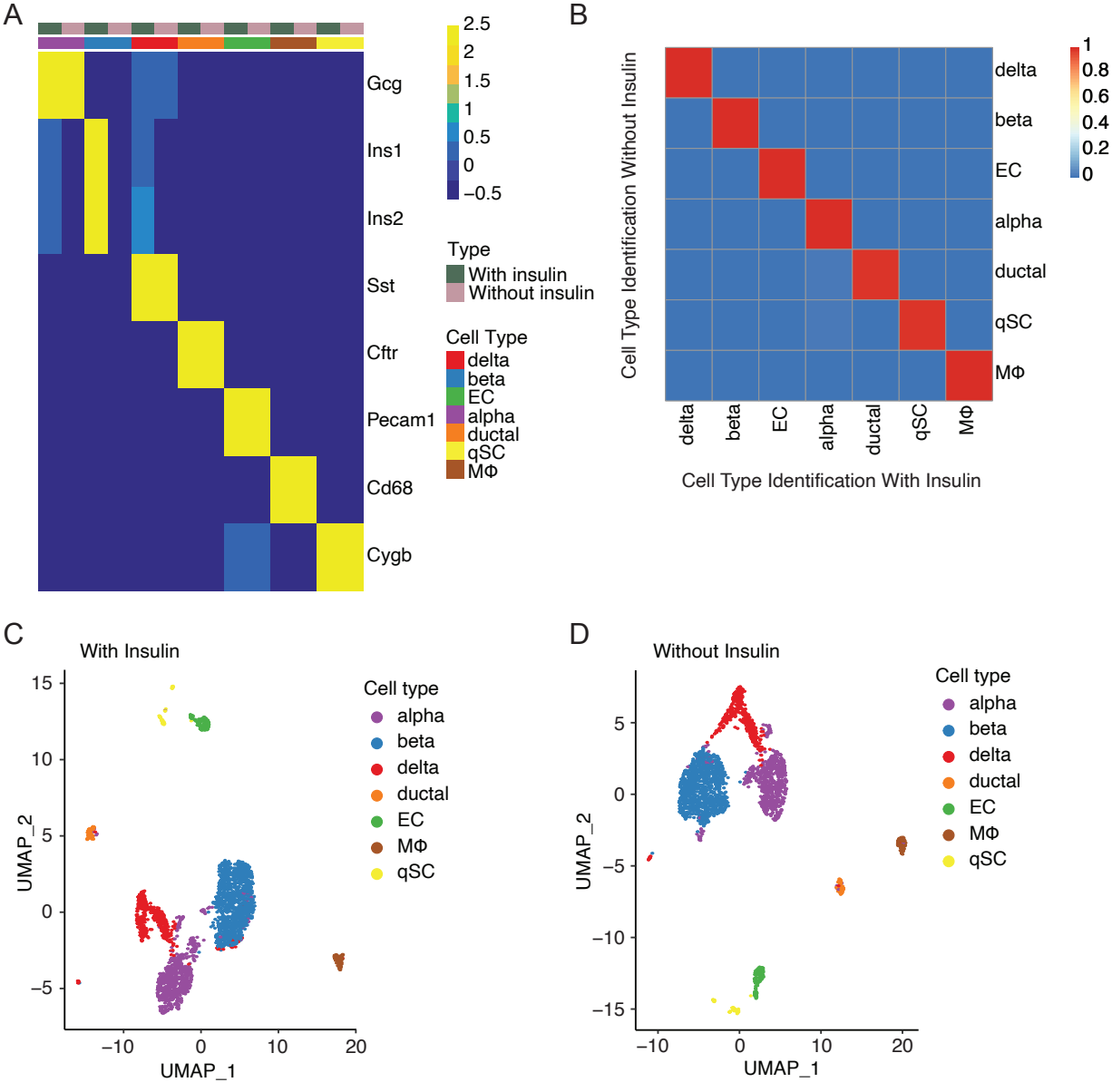

Cell type identification in mouse pancreatic islets with and without insulin transcripts. (A) Heatmap showing expression of cell type–specific markers across clusters defined by gene expression in a dataset including insulin compared to the same dataset from which insulin transcripts have been computationally removed. (B) Confusion matrix comparing cell type assignments between datasets with and without insulin transcripts. (C) UMAP projection of single cells from dataset with insulin, colored by cell type. (D) UMAP projection of single cells from dataset without insulin, colored by cell type.

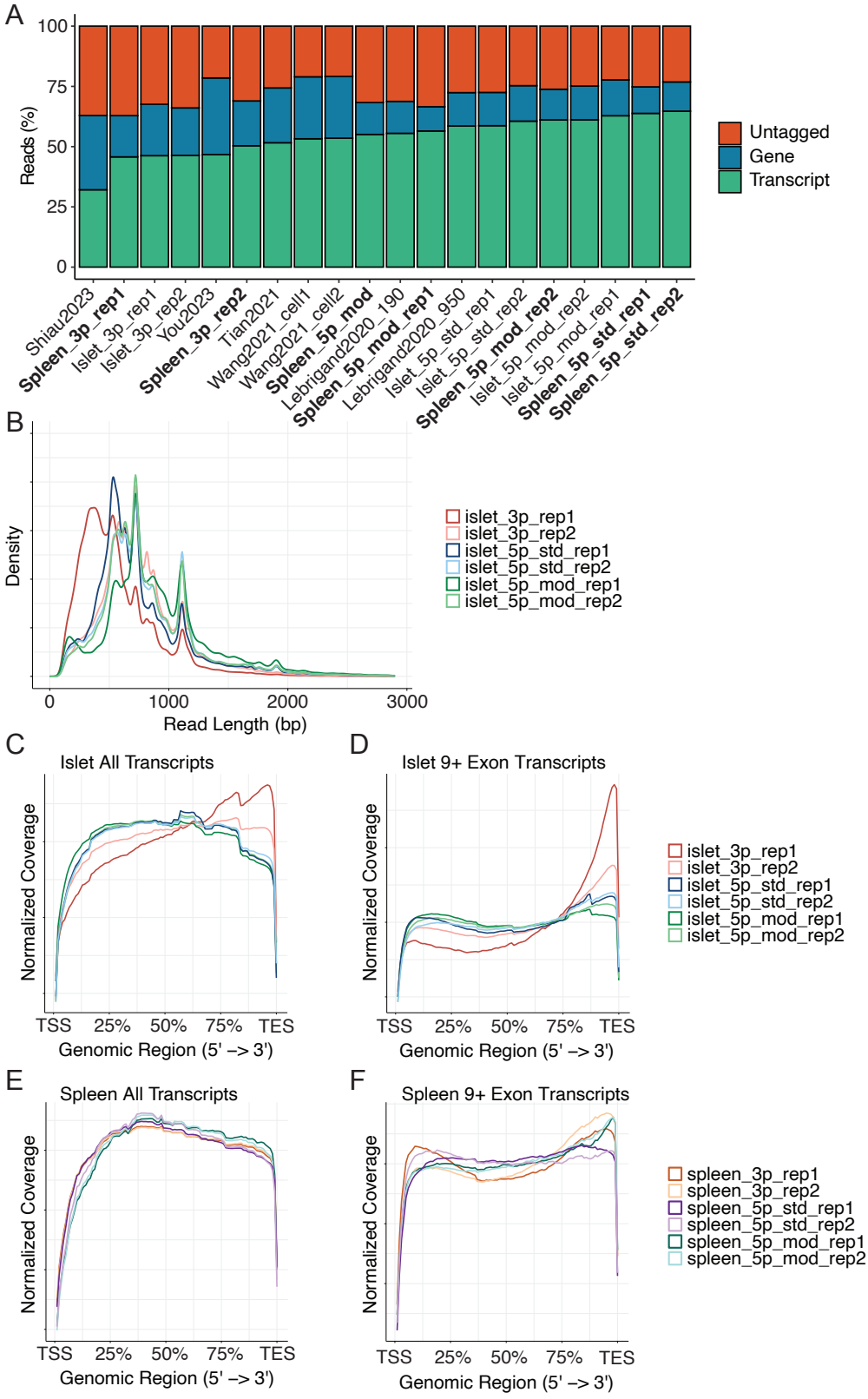

(A) Proportion of reads across datasets where the gene is identified, the transcript is identified, or neither is identified. Shown are six mouse pancreatic islet samples and six mouse spleen samples generated in this study, alongside published reanalyzed datasets. Each tissue from this study includes two biological replicates prepared with 3′ 10x Genomics technology, two with 5′ 10x Genomics technology, and two with 5′ modified 10x Genomics technology. (B) Read length distribution of mouse pancreatic islet scRNA-seq libraries, separated by replicate. Includes two replicates prepared with 3′ 10x Genomics technology, two replicates with 5′ 10x Genomics technology, and two replicates with 5′ 10x Genomics technology with library preparation optimizations. (C–F) Coverage plots showing Softmax-normalized read coverage across relative transcript positions in mouse pancreatic islet (C, D) and spleen (E, F) scRNA-seq libraries prepared with 3′, 5′, or 5′ modified 10x Genomics technology. Samples separated by replicate. Panels C and E include all multi-exon transcripts, while panels D and F include only transcripts with ≥9 exons.

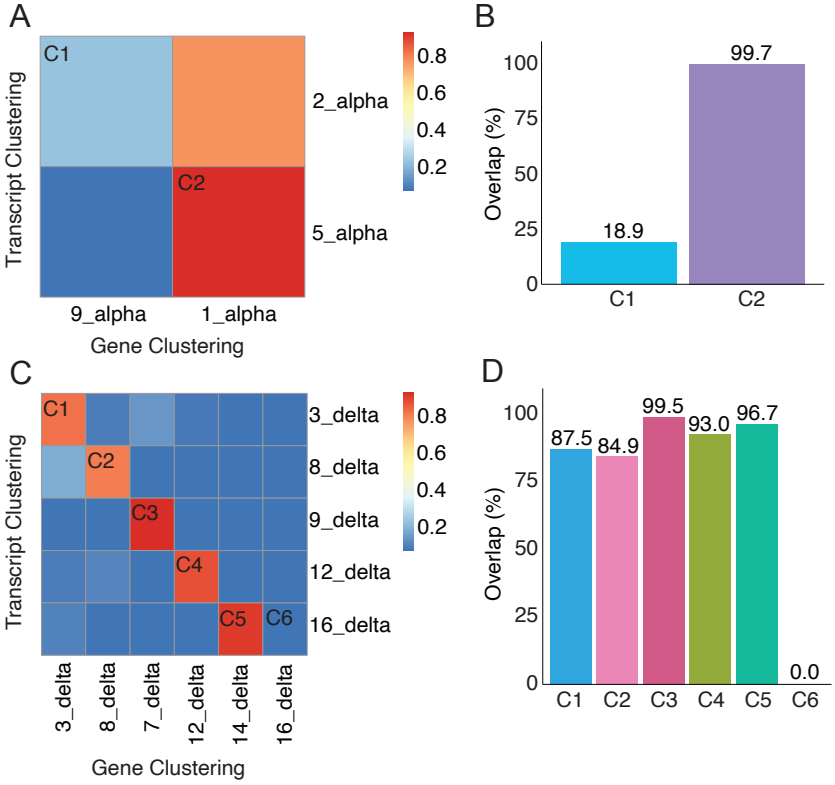

(A) Confusion matrix showing concordance in alpha cell subpopulation identification between gene-based and transcript-based clustering. (B) Bar plot showing concordance of alpha cell subpopulations across clustering methods. Concordance is quantified for two comparisons: C1 (comparison 1) and C2 (comparison 2). (C) Confusion matrix showing low concordance in delta cell subpopulation identification between clustering methods. (D) Bar plot quantifying delta cell subpopulation concordance between clustering methods quantified for comparisons C1-C6.

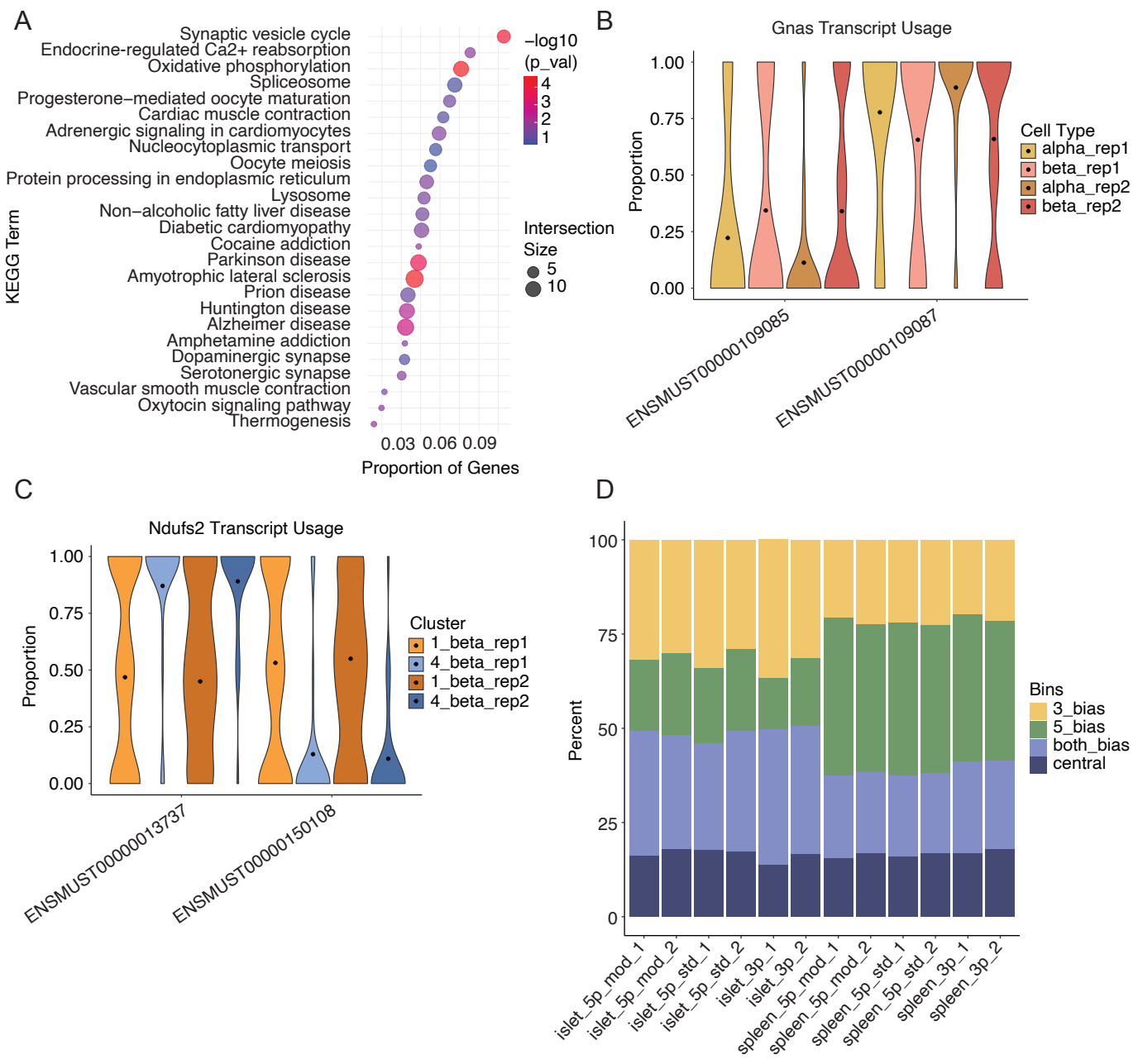

(A) KEGG pathway enrichment for DTU genes between beta cell subpopulations 1_beta and 4_beta. The x-axis shows the proportion of functionally annotated genes in the query that are associated with each pathway. Bubble size represents the number of DTU genes in the pathway, and bubble color indicates statistical significance (-log10 p-value). The top 25 enriched KEGG pathways are shown. (B) Differential transcript usage (DTU) analysis of Gnas between alpha and beta cells, separated by biological replicate. (C) DTU analysis of Ndufs2 between beta cell subpopulations 1_beta and 4_beta, separated by biological replicate. (D) Bar plot showing 3′ versus 5′ bias across libraries prepared with different technologies. Transcripts are classified by whether the junctions that uniquely identify each isoform fall in the 3′ region or 5′ region of the transcript, or both.

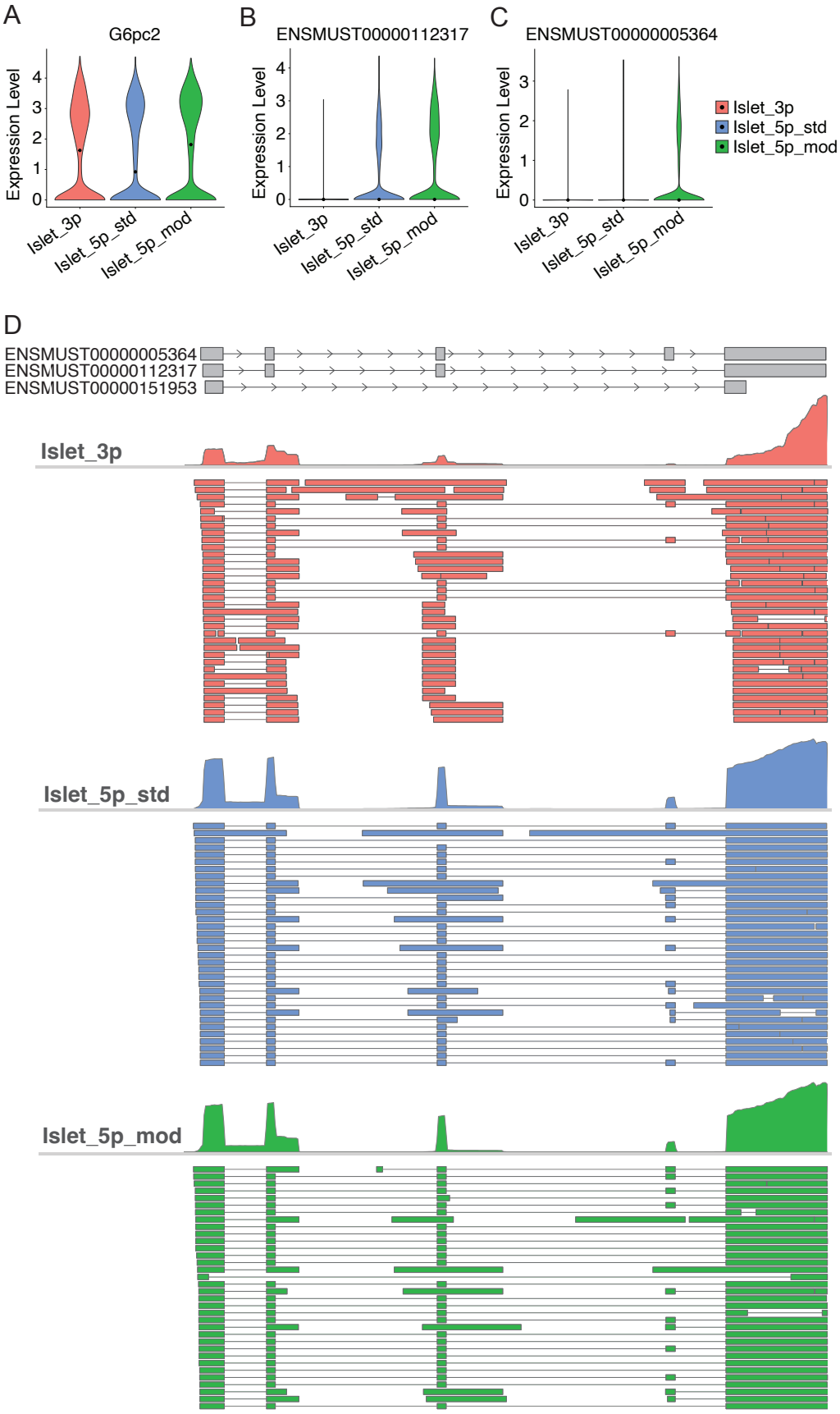

G6pc2 gene and transcript expression across mouse pancreatic islet libraries. (A) Gene-level expression of G6pc2 in 3′ modified, 5′ standard, and 5′ modified libraries (two biological replicates merged for each library). (B) Transcript-level expression of ENSMUST00000112317, isoform of G6pc2, in the same libraries. (C) Transcript-level expression of ENSMUST00000005364, isoform of G6pc2, in the same libraries. (D) Gviz plot showing a gene model track of select transcripts of G6pc2, and an alignments track including all reads uniquely aligned to any transcript of G6pc2.

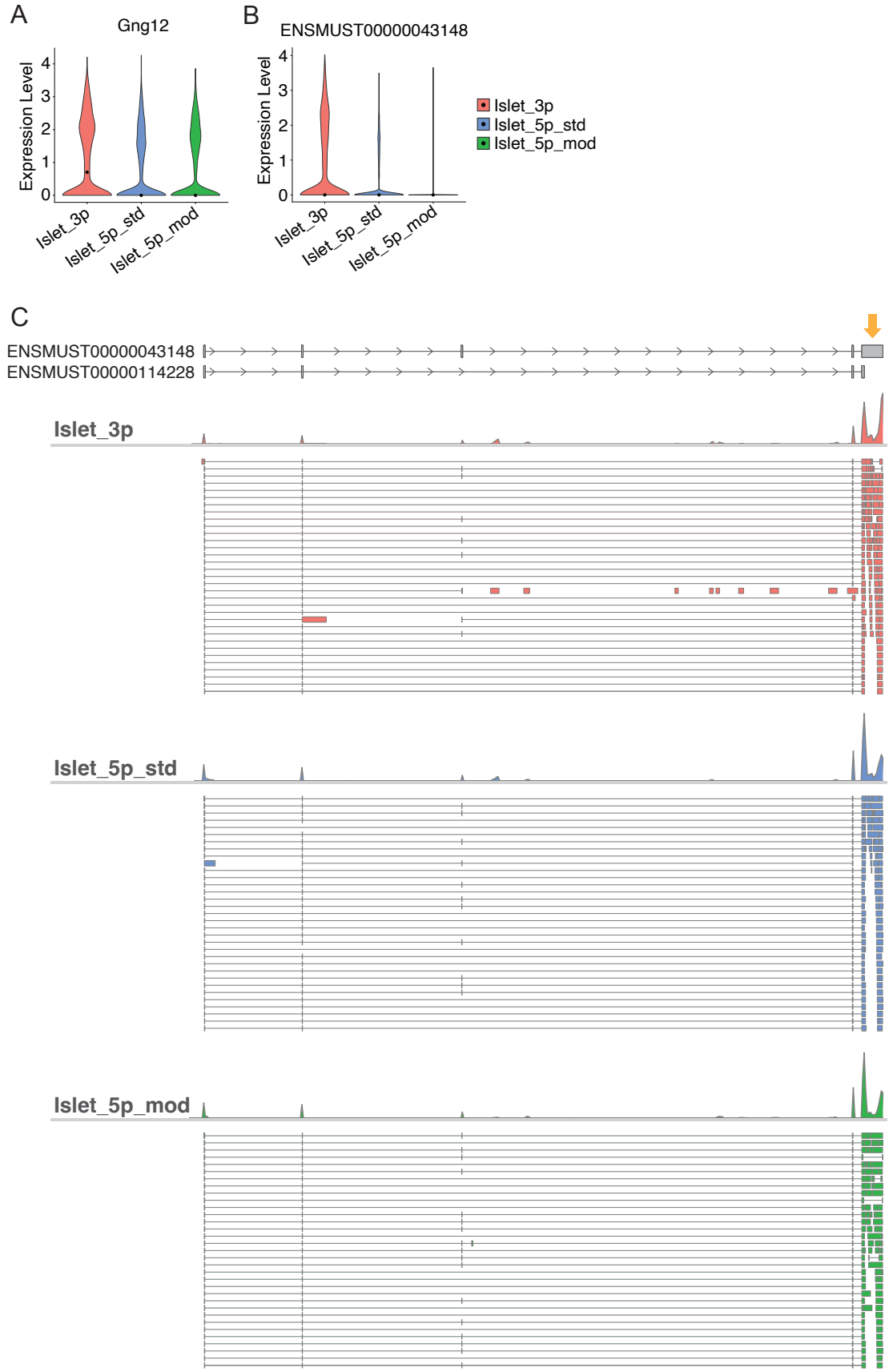

Gng12 gene and transcript expression across mouse pancreatic islet libraries. (A) Gene-level expression of Gng12 in 3′ modified, 5′ standard, and 5′ modified libraries (two biological replicates merged for each library). (B) Transcript-level expression of ENSMUST00000043148, isoform of Gng12, in the same libraries. (C) Gviz plot showing a gene model track of select transcripts of Gng12, and an alignments track including all reads uniquely aligned to any transcript of Gng12. Arrow indicates a long exon at the 3' end of the transcript.

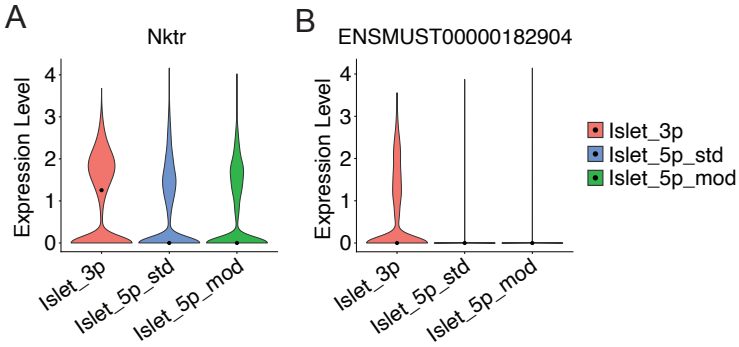

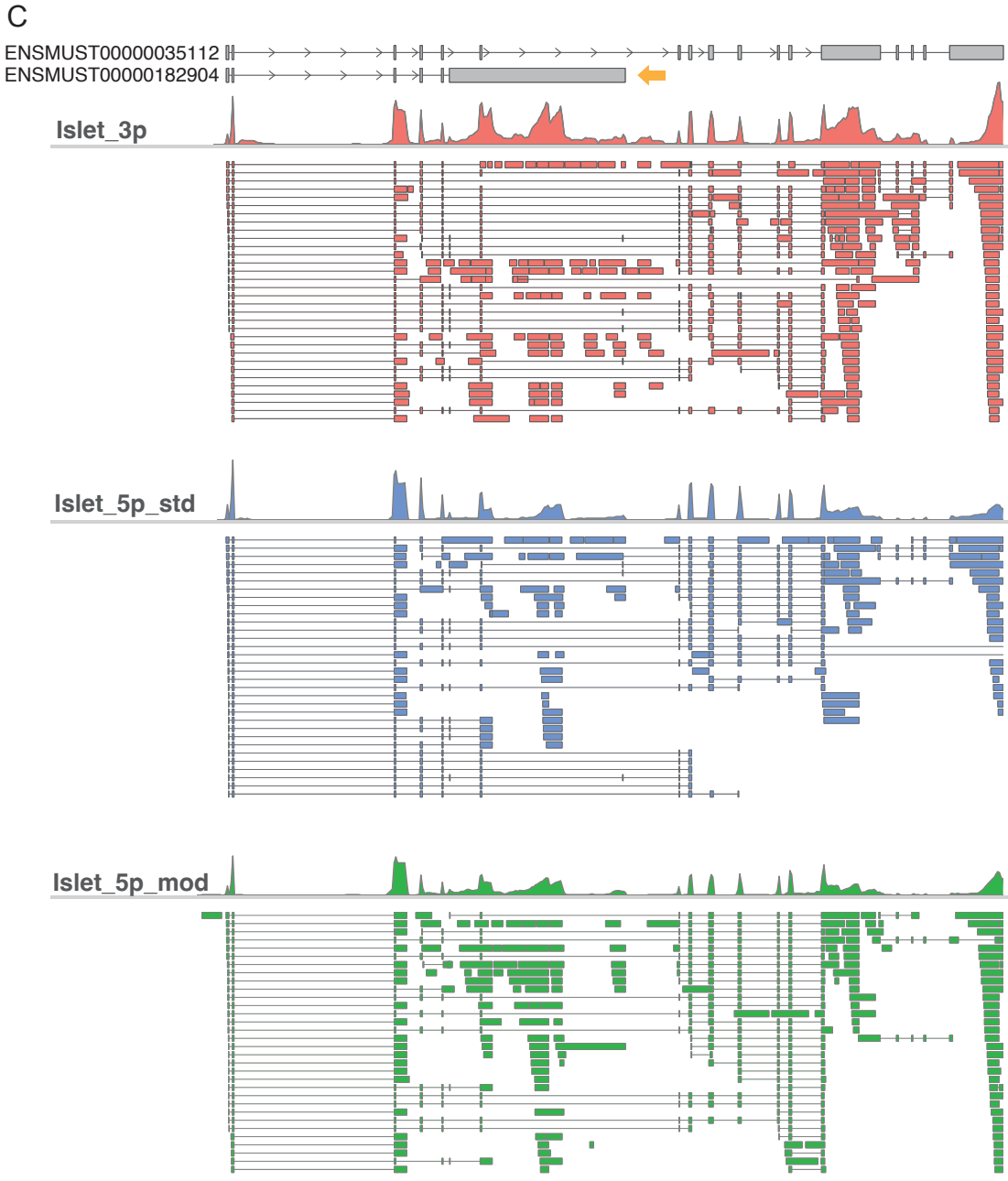

Nktr gene and transcript expression across mouse pancreatic islet libraries. (A) Gene-level expression of Nktr in 3′ modified, 5′ standard, and 5′ modified libraries (two biological replicates merged for each library). Transcript-level expression of ENSMUST00000182904, isoform of Nktr, in the same libraries. (C) Gviz plot showing a gene model track of select transcripts of Nktr, and an alignments track including all reads uniquely aligned to any transcript of Nktr. Arrow indicates retained intron captured by internal priming.

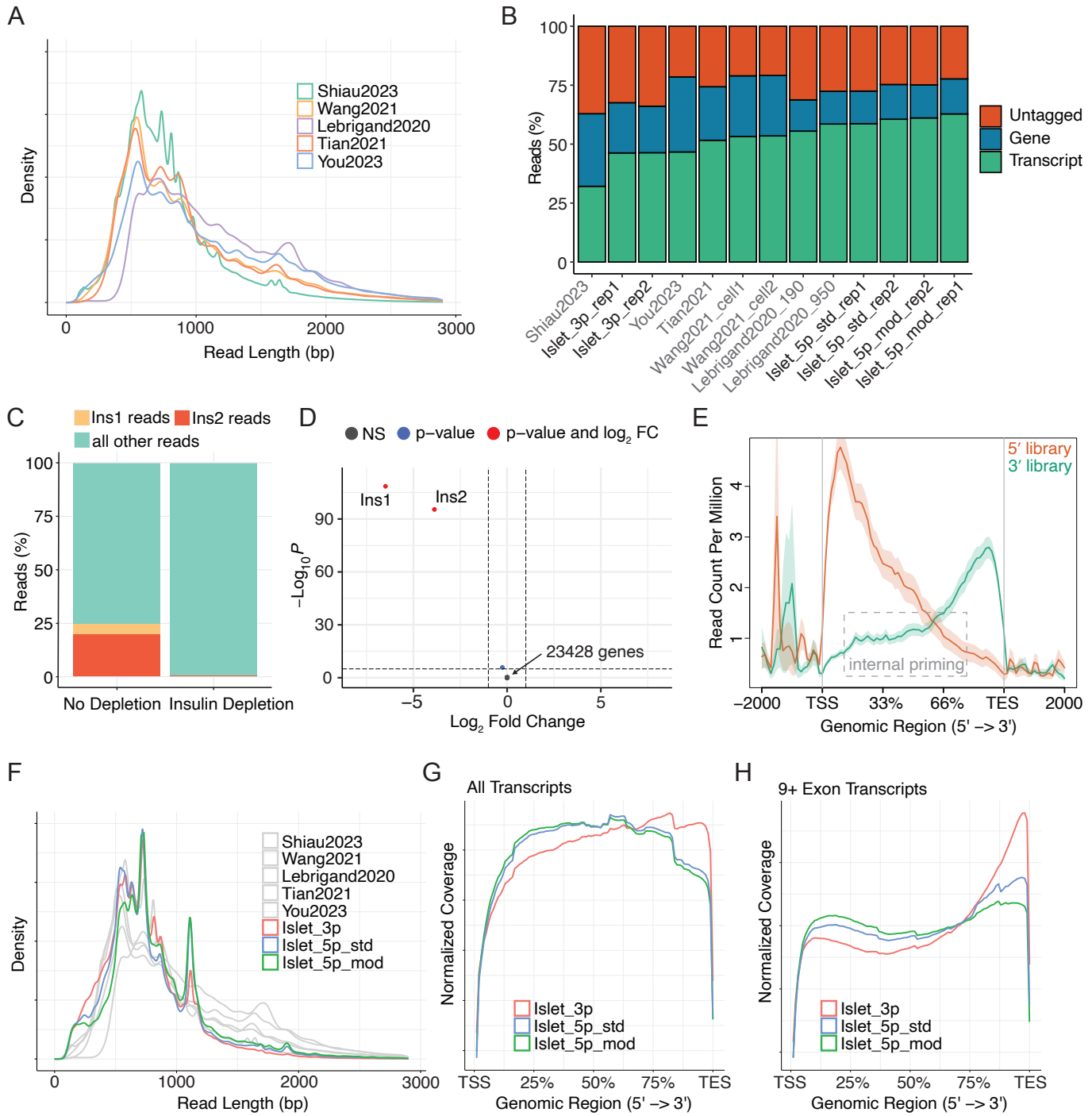

Read length and transcript identification comparison between single-cell long-read RNA-sequencing (sclrRNA-seq) libraries. (A) Read length distribution of published sclrRNA-seq libraries prepared with 10x Genomics and Nanopore technology. Biological replicates are merged for datasets from Lebrigand et al., 2020 and Wang et al., 2021; other datasets are shown as single samples. (B) Proportion of reads across datasets where the gene is identified, the transcript is identified, or neither is identified. Shown are published reanalyzed datasets and six mouse pancreatic islet samples: two replicates prepared with 3′ 10x Genomics technology, two replicates with 5′ 10x Genomics technology, and two replicates with 5′ 10x Genomics technology incorporating library preparation optimizations. (C) Proportion of reads aligned to Ins1 or Ins2 in a single-cell RNA-seq analysis of mouse pancreatic islets pre- and post-insulin depletion. (D) Volcano plot depicting differential gene expression between non-depleted and insulin-depleted bulk RNA-seq libraries from mouse pancreatic islets. A total of 23,431 genes is shown in the plot. (E) NGS coverage plot indicating read start sites across the genomic region. Libraries shown are 3′ and 5′ single-cell 10x Genomics preparations from human DTC melanoma cells. (F) Read length distribution comparison across mouse pancreatic islet scRNA-seq libraries, including two replicates prepared with 3′ 10x Genomics technology, two replicates with 5′ 10x Genomics technology, and two replicates with 5′ 10x Genomics technology with library preparation optimizations, alongside published scRNA-seq datasets. Biological replicates are merged for the 10x libraries as well as for datasets from Lebrigand et al., 2020 and Wang et al., 2021. (G) Coverage plot showing Softmax-normalized read coverage across relative transcript positions for all multi-exon transcripts in mouse pancreatic islet scRNA-seq libraries prepared with 3′, 5′, or 5′ modified 10x Genomics technology. (H) Coverage plot showing Softmax-normalized read coverage across relative transcript positions for all transcripts with ≥9 exons in mouse pancreatic islet scRNA-seq libraries prepared with 3′, 5′, or 5′ modified 10x Genomics technology.

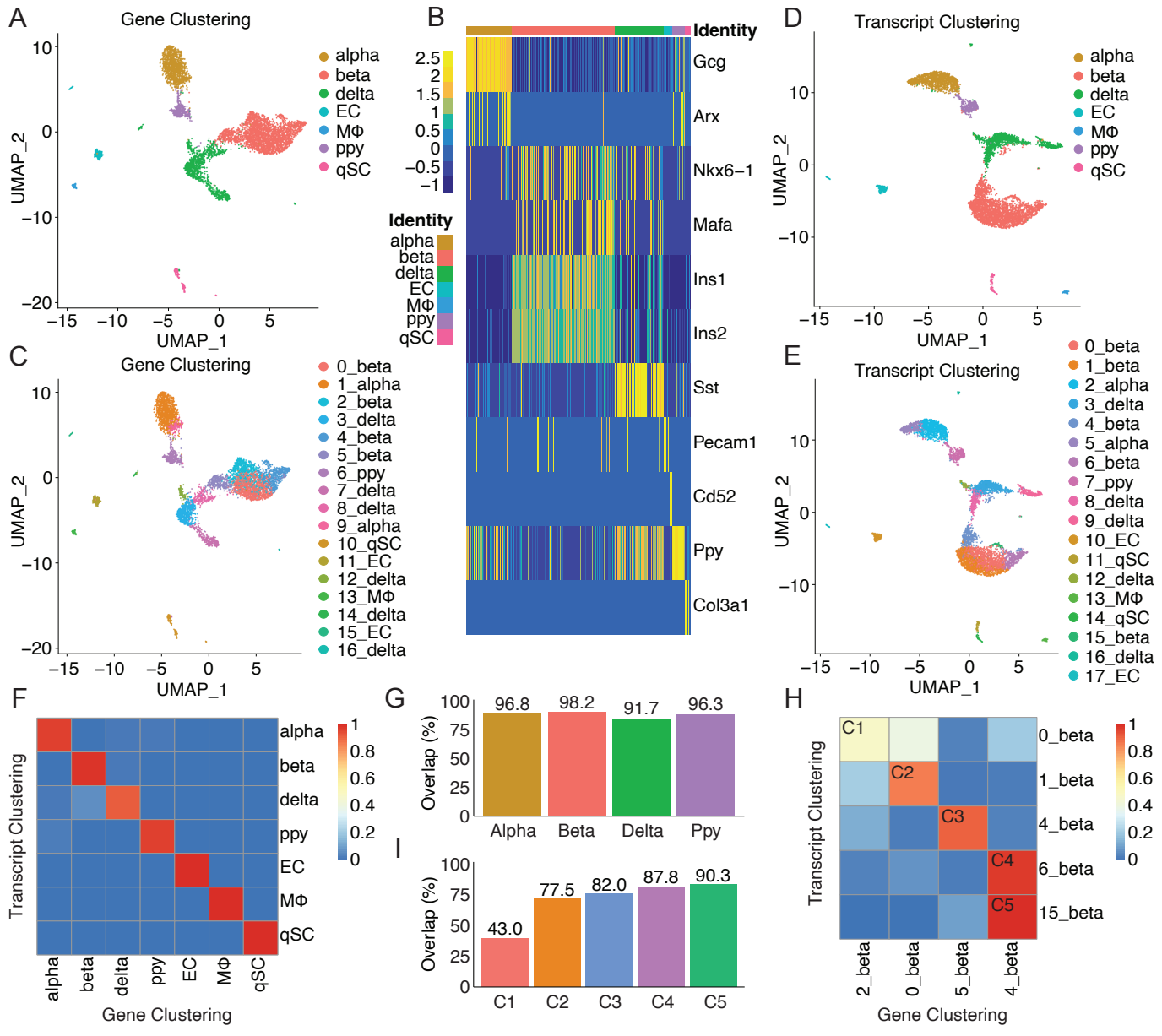

Comparison of single-cell clustering based on gene expression versus transcript-level expression. (A) UMAP projection of single cells from insulin-depleted mouse pancreatic islet sclrRNA-seq libraries prepared with 5′ modified 10x Genomics technology (two biological replicates merged). Cells are colored by gene expression profiles reflecting major pancreatic cell types. (B) Heatmap showing expression of cell type–specific markers across insulin-depleted 5′ modified libraries (two biological replicates merged), based on gene-level clustering. Cell type abbreviations: EC, endothelial cell; MΦ, macrophage; qSC, quiescent stellate cell. (C) UMAP projection of single cells based on gene-level expression, colored by gene expression profiles reflecting cell subpopulations. (D) UMAP projection of single cells based on transcript-level (isoform) expression. Colored by transcript expression profiles reflecting major pancreatic cell types. (E) UMAP projection of single cells based on transcript-level expression, grouped by transcript expression profiles reflecting cell subpopulations. (F) Confusion matrix showing concordance in cell type identification between gene-based and transcript-based clustering. (G) Bar plot quantifying cell type concordance between clustering methods. (H) Confusion matrix showing low concordance in beta cell subpopulation identification between clustering methods. (I) Bar plot quantifying beta cell subpopulation concordance between clustering methods. C1–C5 indicate comparison 1 through comparison 5.

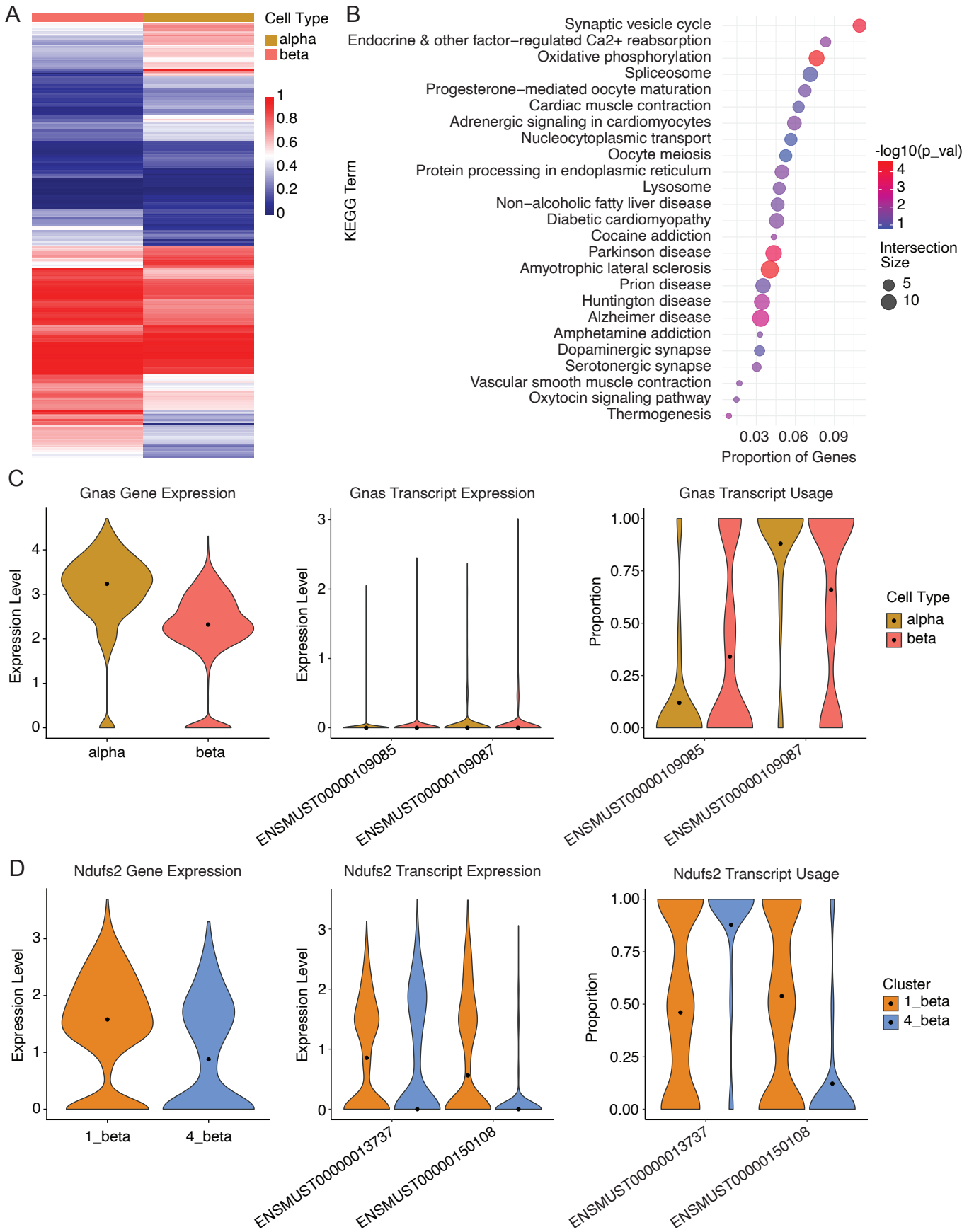

Differential transcript usage between cell types and cell subpopulations. (A) Heatmap showing differential transcript usage (DTU) between alpha and beta cells. Each row represents a transcript (significant at FDR < 0.05), and each column represents a cell type. Colors indicate the fraction of a gene's expression contributed by each transcript within each cell type. DTU genes were identified from pseudobulk analysis of two biological replicates of mouse pancreatic islet sclrRNA-seq libraries prepared with 5′ modified 10x Genomics technology. (B) KEGG pathway overrepresentation analysis (ORA) for DTU genes between alpha and beta cells. The x-axis shows recall, i.e., the proportion of functionally annotated genes in the query that are associated with each pathway. Bubble size represents the number of DTU genes in the pathway, and bubble color indicates statistical significance (-log10 p-value). The top 25 enriched KEGG pathways are shown. (C) Differential gene expression (DGE), differential transcript expression (DTE), and differential transcript usage (DTU) analysis of Gnas between alpha and beta cells. DTU shows the relative contribution of each transcript to the gene's overall expression. (C) DGE, DTE, and DTU analysis of Ndufs2 between beta cell subpopulations 1_beta and 4_beta.